AMERICAN COLLEGE of SPORTS MEDICINE
LEADING THE WAY

. . . Published ahead of Print

3D Tibial Acceleration and Consideration of 3D Angular Motion Using IMUs on Peak Tibial Acceleration and Impulse in Running

Robbert P. van Middelaar[1], Junhao Zhang[1], Peter H. Veltink[1], and Jasper Reenalda[1,2]

[1]University of Twente, Enschede, THE NETHERLANDS; [2]Roessingh Research & Development, Enschede, THE NETHERLANDS

Accepted for Publication: 20 July 2023

Medicine & Science in Sports & Exercise, Publish Ahead of Print
DOI: 10.1249/MSS.0000000000003269

3D Tibial Acceleration and Consideration of 3D Angular Motion Using IMUs on Peak Tibial Acceleration and Impulse in Running

Robbert P. van Middelaar[1], Junhao Zhang[1], Peter H. Veltink[1], and Jasper Reenalda[1,2]

[1]University of Twente, Enschede, THE NETHERLANDS; [2]Roessingh Research & Development, Enschede, THE NETHERLANDS

Address for Correspondence: Robbert Pieter van Middelaar, University of Twente, Drienerlolaan 5, Enschede, Overijssel 7522NB, The Netherlands; E-mail: r.p.vanmiddelaar@utwente.nl; Phone: +31 534894687

Conflict of Interest and Funding Source:

This project is funded by a general research fund of the University of Twente, Enschede, The Netherlands. All authors declare no conflict of interest. The results of the study are presented clearly, honestly, and without fabrication, falsification, or inappropriate data manipulation. The results of the present study do not constitute endorsement by the American College of Sports Medicine.

ABSTRACT

Purpose: Peak tibial acceleration (PTA) is defined as the peak acceleration occurring shortly after initial contact, often used as an indirect measure of tibial load. As the tibia is a rotating segment around the ankle, angular velocity and angular acceleration should be included in PTA. This study aimed to quantify 3D tibial acceleration components over two different sensor locations and three running speeds, to get a better understanding of the influence of centripetal and tangential accelerations on PTA typically measured in running. Furthermore it explores tibial impulse as alternative surrogate measure for tibial load. **Methods:** 15 participants ran 90 seconds on a treadmill at 2.8, 3.3, and 3.9 $m \cdot s^{-1}$, with IMUs located distally and proximally on the tibia. **Results:** Without the inclusion of rotational accelerations and gravity, no significant difference was found between axial PTA between both IMU locations, while in the tangential sagittal plane axis there was a significant difference. Inclusion of rotational accelerations and gravity resulted in similar PTA estimates at the ankle for both IMUs, and caused a significant difference between PTA based on the distal IMU and PTA at the ankle. The impulse showed more consistent results between the proximal and distal IMU location compared to axial PTA. **Conclusions:** Rotational acceleration of the tibia during stance differently impacted PTA measured proximally as well as distally at the tibia, indicating that rotational acceleration and gravity should be included in PTA estimates. Furthermore, peak acceleration values (such as PTA) are not always reliable when using IMUs due to inconsistent PTA proximally compared to distally on an individual level. Instead, impulse seems to be a more consistent surrogate measure for the tibial load.

Key Words: CENTRIPETAL, TANGENTIAL, GRAVITATIONAL, TIBIAL LOAD

INTRODUCTION

Running ten kilometers could comprise over several thousand ground contacts, resulting in significant repetitive impacts on the body while landing on the ground (1). Peak tibial acceleration (PTA) is often used as an indirect measure for the impact load at the tibia (2–6), and several studies link increased PTA to injuries retrospectively (7,8). PTA plays a role in the internal bone loading even though there is no direct relation between externally measure PTA and the internal tibial bone loading (9,10). Other factors like for instance the muscle forces acting on tibia and the bending of the tibia under impact play an important role as well (11–13). Nevertheless, PTA is an easy to use and frequently measured parameter that can help better understand the load on the tibia during running. PTA is defined as the peak axial acceleration value at the tibia occurring shortly after initial contact, commonly measured with an accelerometer (14). PTA typically varies between approximately 2g and 12g, but is highly dependent on factors such as foot strike pattern and orientation and movement of the tibia, stride frequency, running surface, but also sensor location and running speed (14).

Even though the tibia is often considered a rigid body, the location of the sensor at the tibia influences PTA (14–17). As the tibia is a rotating segment around the ankle joint during stance, acceleration measured by an accelerometer does not only consist of acceleration caused by impact with the ground (18). One needs to take into account gravitational acceleration, but also location-dependent rotational accelerations like centripetal and tangential acceleration. However, this is often not complied with because the typically used accelerometers cannot measure the kinematics needed to assess gravitational, centripetal, and tangential acceleration (14,15,17). The generally used assumption that PTA can be measured with an accelerometer

anywhere on the tibia, since the tibia is a rigid body, is not correct because distal and proximal peak acceleration measured by an accelerometer differ significantly (6,14,16,17).

Centripetal and tangential acceleration are evaluated by the angular velocity and angular acceleration of the tibia, respectively, and the distance from the sensor to the ankle joint (18,19). As a consequence, centripetal and tangential acceleration are larger further away from the ankle joint, which causes the accelerometer output to differ at different locations across the entire tibia (18). However, sensors are placed at various locations in running studies (14): ranging from 2 to 4 cm (20), 8 cm (21), or 12 cm (22) above the medial malleolus towards placing a sensor on the proximal anteromedial aspect of the tibia (2,5,23). Therefore, it can be expected that different sensor locations will result in different, and incomparable, PTA values due to the rotational motion of the tibia. In order to correctly evaluate the role of PTA in tibial bone loading and to compare PTA values measured at different locations, they need to be corrected for angular motion and gravitational aspects.

To get a better understanding of the effects of angular motion and gravitational aspects on PTA and its role in tibial bone loading running speeds needs to be evaluated, since running speed affects peak accelerations (14), angular velocity, and angular acceleration during stance. Peak accelerations increase non-linearly with higher running speed (14), approximately 34 to 42% per 1 $m \cdot s^{-1}$ (24,25). Running speed will therefore have an influence on the angular velocity of the tibia during stance and consequently on the PTA values, due to faster movement of the leg at higher speeds, with consequently higher initial impact velocity and greater rates of dorsiflexion around the ankle. This likely increased angular velocity of the tibia segment. Hence, running

speed is an important factor in peak impact acceleration, as well as in centripetal and tangential acceleration contributions (24,25). As a result, PTA based only on an accelerometer may not always be correctly interpreted or comparable over different running speeds while ignoring the centripetal and tangential acceleration. Corrections for these changing angular motions might allow PTA values to be compared at different running speeds.

In previous work, Lafortune and Hennig (18) used high-speed video recording to estimate centripetal acceleration during running, and showed that this could be as high as 50 $m \cdot s^{-2}$ proximally at the tibia (18). In other studies, significant differences between distal and proximal PTA estimates were found (6,16,17). However, only accelerometers were used in these studies, and therefore it was not possible to take into account the contribution of the centripetal and tangential components. Lake et al. (2005) (22) did assess the contribution of the centripetal component in PTA and concluded that centripetal acceleration needs to be taken into account when interpreting tibial impact. However, they did not investigate PTA at different speeds and used an optical motion capture system in a lab to estimate centripetal acceleration instead of inertial measurement units (IMUs). IMUs are convenient sensors for this application, as they measure acceleration and angular velocity simultaneously, are easy to use, and not bound to a lab (26). As such, they can provide information about the impact acceleration solely caused by the impact from the ground by taking into account the rotational acceleration. When these rotational accelerations are taken into account, the measured acceleration are theoretically moved to the ankle joint (as the origin of the rotations during stance). Since the ankle joint axis is not obvious to locate from the exterior, the medial malleolus is a practical-to-use surrogate for the ankle joint, taking into account a slight translation. The recommendation to include centripetal and tangential

accelerations in PTA estimates (18,22) is still not common practice, but it is needed to obtain a consistent PTA estimate at the ankle joint. The resulting PTA at the ankle joint is then independent of sensor location, and valid over varying running speeds.

Investigating a single peak value, like PTA, is highly dependent on a sufficient sample frequency of the IMU in order not to miss the exact peak (27). Typically, the IMU sample frequency is lower compared to an accelerometer (14). The question rises if PTA based on a single sample obtained with an IMU is an appropriate measure or if a more robust method to obtain consistent and accurate estimates of the impact is needed. The mechanical impulse is used more often for impact evaluation with, for example, force plate data (28) or pressure insoles (29,30), but also the time integral of foot acceleration curves can be used as impulse (31). The impulse takes into account the magnitude, but also the time duration of the impact and is therefore evaluating impact not only at the peak value, but during the entire impact wave. The impulse could therefore be a more appropriate surrogate measure for the external load on the tibia during the impact phase using IMUs, while still taking into account angular velocity and angular acceleration.

Assessment of 3D PTA including centripetal, tangential, and gravitational acceleration over different sensor locations and speeds has not been considered yet, but may provide relevant information about the total contribution of the acceleration caused by ground impact at the tibia. Furthermore, the investigation of the single-valued PTA estimate versus the impulse could give insight whether PTA estimates should still be used in biomechanics research, or other surrogate measures are more appropriate. This study aims to quantify all 3D tibial acceleration components

over two different sensor locations on the tibia and three running speeds (2.8, 3.3, and 3.9 $m \cdot s^{-1}$), to explore the contribution of centripetal and tangential accelerations in PTA. Furthermore, the tibial acceleration is evaluated with the more robust estimate of the impulse while using an IMU.

It is hypothesized that PTA measured using an accelerometer at the tibia differs significantly from PTA values transferred to the ankle when taking into account the rotational components. In addition, it is expected that PTA at the ankle shows a greater increase with increasing running speeds compared with PTA measured using an accelerometer on a certain distance from the ankle, caused by the contributions of centripetal and tangential accelerations. Furthermore, it is expected that an impulse-based measure of tibial acceleration can give a more consistent measure of the external impact on the tibia compared to a single-valued PTA estimate. This underlines that PTA, measured by accelerometers, seems to have a doubtful future as a surrogate measure for tibial bone load.

METHODS

This study was part of a larger project, but only the relevant parts for this research are described here.

Participants

15 recreational runners (10M/5F, 31.7 ±9.9 yrs, 182.1 ±9.6 m, 76.3 ±16.1 kg, 13 right dominant, 2 left dominant, distance of distal IMU from ankle 11.3 ±2.3 cm, distance of proximal IMU from ankle 30.7 ±3.2 cm, tibia length 43.9 ±2.9cm) were included in this study. They ran recreationally (> 15 kilometres per week on average, for at least 6 months) and had a self-

reported habitual rearfoot strike (RFS) pattern. They were able to run 3.9 $m \cdot s^{-1}$ for at least 5 minutes. They reported no major injuries in the past six months, and had some experience with treadmill running. The local ethics committee (University of Twente, EEMCS EC-CIS; ref: RP2021-117) approved the experimental protocol of this study. All participants signed written informed consent. 18 participants volunteered to join this study. Three participants were excluded because of a clear forefoot strike, malfunction of IMUs, or because they were not able to finish the complete protocol.

Measurement devices

The protocol was performed on one side of a split-belt treadmill (custom Y-mill, Motek, Culemborg, The Netherlands) with an embedded 3D force plate (sampling at 1024 or 2048 Hz). Three IMUs (dimensions 36 x 24.5 x 10 mm, mass 10 g) (Xsens MVN Link, Xsens Technologies BV, Enschede, the Netherlands) measured angular velocity (range ± 2000°/s) and acceleration (range ± 16 g) with a sampling rate of 240 Hz. Two IMUs were placed on the tibia of the dominant leg, distally and anteromedially (11.3 ± 2.3 cm above the medial malleolus, see Figure 1) and proximally on the anteromedial surface of the tibia (30.7 ± 3.2 cm above the medial malleolus, see Figure 1), respectively. A third IMU was located proximally on the anteromedial surface of the non-dominant tibia, used for time-synchronization (see 2.4). IMUs were attached to the skin with double-sided skin-friendly tape and were covered by a layer of strapping tape. The participant wore compressing socks over the tibia to minimize movement of the tibia IMUs following the method proposed by (32). The lower extremity kinematics were recorded in the sagittal plane with a camera on a tripod (JVC GC-PX100BE, Yokohama, Japan).

Experimental design

Foot strike pattern (FSP) was recorded with the video camera during all trials. RFS was defined as the rear end of the shoe hitting the ground first. If the participant had a confirmed RFS on video, the participant was included in the study. Only rearfoot striking participants were included to eliminate the effect of FSP on PTA (33).

Anthropometric measurements of the foot and tibia were performed and the dominant leg was determined by asking the participant with which leg they would kick a ball (34). Only the dominant leg was evaluated to avoid inclusion of any asymmetric behaviour of the legs in the analysis (35). Before the measurement, participants performed a self-chosen warming-up. Participants ran for 90 seconds at 3 different speeds (2.8, 3.3, 3.9 $m \cdot s^{-1}$) in randomized order on their preferred stride frequency, with at least a 3-minute rest in between each trial to minimize fatigue.

Data processing

Xsens software (Xsens MVN Analyze Pro 2021.0.1) was used to acquire data from the IMUs. Angular velocity and acceleration were directly obtained from the IMUs, without calibration or alignment with an anatomical coordinate system. MATLAB (MathWorks Inc., Natick, MA, USA, version 2021b) was used for data processing.

3D sensor accelerations and 3D sensor angular velocity were acquired from the IMUs (240 Hz). IMU data were obtained in a proximal (Ψ_{IMU_p}) or distal (Ψ_{IMU_d}) IMU-dependent coordinate system (CS), with z-axis pointing upwards, x-axis frontally, and y-axis to the left in

the IMU frame to fit a right-handed CS (see both CS on the left in Figure 1). Ψ_{IMU_p} was rotated with a time-independent rotation matrix based on principal component analysis (PCA) of the 3D IMU angular velocity of the entire trial (36)**.** This creates a functional axis perpendicular to the sagittal plane movement of the tibia, to have IMU data with the y-axis always as main rotational axis. This allows movement of the IMU with the tibia mainly in the sagittal plane to form a functional IMU-dependent CS: $\Psi_{IMU_{p_f}}$. The same method was applied to Ψ_{IMU_d} to obtain $\Psi_{IMU_{d_f}}$ (see CS on the right in Figure 1).

Vertical ground reaction force (vGRF) was obtained from the force plate (FP), and was down-sampled towards 240 Hz from 1024 or 2048 Hz (depending on force plate settings) to match IMU sample frequency. Time-synchronization of both systems was done with three vertical jumps at the start and end of each trial. Axial acceleration (including gravity) of the left and right proximal tibia IMU during the first three jumps were used for normalized cross-correlation with the vGRF of the FP. Three jumps at the end of the trial were used to check this time-synchronization, where FP data was interpolated to compensate for a potential mismatch of the internal clocks of the FP and IMU system.

Angular acceleration was obtained as the time derivative of angular velocity. Angular velocity and angular acceleration were filtered with a zero-phase 2nd order Butterworth filter. A cut-off frequency of 30 Hz was used for the angular velocity data, based on (37). Angular acceleration was filtered with a cut-off frequency of 15 Hz, based on (18). Sensor acceleration and FP data were filtered with a zero-phase 2nd order Butterworth filter with a cut-off frequency of 60 Hz according to (18).

30 strides were obtained halfway through the 90-second run at each speed and these were used in further processing. Initial contact (IC) and toe-off (TO) were determined when the vGRF measured by the FP exceeded or fell below 30 N, respectively. The distance from the medial malleolus towards the distal or proximal IMU origin was measured with measure tape, but if not available, the distance was estimated with the video recording where the participant was standing still. The shoe length (in cm) and height of the lateral malleolus to the floor (in cm) were measured with measure tape. These distances were used in the video recording to estimate the distance from the medial malleolus to IMU.

The determination of the gravitational acceleration and the alignment of $\Psi_{IMU_{p_f}}$ and $\Psi_{IMU_{d_f}}$ can be found in the Supplemental Digital Content (see text, Supplemental Digital Content, Gravitational acceleration determination & alignment of $\Psi_{IMU_{p_f}}$ and $\Psi_{IMU_{d_f}}$, http://links.lww.com/MSS/C891). $\Psi_{IMU_{p_f}}$ and $\Psi_{IMU_{d_f}}$ are now assumed identical over time and defined as Ψ_{IMU_f} in the remainder of this paper.

Parameters

PTA and its components (3D). *With Rigid Body Kinematics (RBK) one can obtain the acceleration on a specified location on a rigid body based on the kinematics measured by a body-mounted IMU (19,38), using Equation 1:*

$$\vec{\boldsymbol{a}}_2 = \vec{\boldsymbol{a}}_1 + \vec{\boldsymbol{\alpha}} \times \vec{\boldsymbol{r}}_{1\to 2} + \vec{\boldsymbol{\omega}} \times (\vec{\boldsymbol{\omega}} \times \vec{\boldsymbol{r}}_{1\to 2}) \qquad [1]$$

Where $\vec{\boldsymbol{a}}_2$ is the estimated acceleration (m·s^{-2}) on a specified location, $\vec{\boldsymbol{a}}_1$ is the IMU-measured acceleration (m·s^{-2}). Angular acceleration, $\vec{\boldsymbol{\alpha}}$ (rad/s^2), is the time derivative of the angular velocity measured by the IMU, $\vec{\boldsymbol{\omega}}$ (rad/s). $\vec{\boldsymbol{r}}_{1\grave{a}2}$ (m) is the 3D position vector from the IMU location towards a specified location.

Equation 1 forms the base to translate the acceleration measured with an IMU (i.e., $\vec{\boldsymbol{a}}_1$) to the ankle joint (i.e., $\vec{\boldsymbol{a}}_2$) for both IMUs. One can derive three distinctive equations for the acceleration estimate at the ankle joint for each axis in Ψ_{IMU_f}: tangential in sagittal plane (x-axis in Ψ_{IMU_f}, Equation 2), tangential in the frontal plane (y-axis in Ψ_{IMU_f}, Equation 3), and axially (z-axis in Ψ_{IMU_f}, Equation 4):

$$a_{free,ankle_x}(t) = (a_{IMU_x}(t) - g_x(t)) - \alpha_y(t)\, r_z \quad [2]$$

$$a_{free,ankle_y}(t) = (a_{IMU_y}(t) - g_y(t)) - \alpha_x(t)\, r_z \quad [3]$$

$$a_{free,ankle_z}(t) = (a_{IMU_z}(t) - g_z(t)) + \omega_y^2(t)\, r_z + \omega_x^2(t)\, r_z \quad [4]$$

With $\overrightarrow{\boldsymbol{a_{free,ankle}}}$ (m·s^{-2}) as the gravity-free acceleration at the ankle joint, $\overrightarrow{\boldsymbol{a_{IMU}}}$ (m·s^{-2}) as IMU-measured acceleration, and $\vec{\boldsymbol{r}}$ (m) as distance between the IMU and the medial malleolus. Centripetal acceleration is defined as $\overrightarrow{\boldsymbol{\omega^2\, r}}$ (m·s^{-2}), tangential acceleration as $\overrightarrow{\boldsymbol{\alpha\, r}}$ (m·s^{-2}), and gravitational acceleration as $\vec{\boldsymbol{g}}$ (m·s^{-2}). Radius $\vec{\boldsymbol{r}}$ was only evaluated in the axial direction (z-axis in Ψ_{IMU_f}), due to assumed negligible contributions of r_x and r_y.

PTA_{ankle_z} was taken as the peak value of the $a_{free,ankle_z}$ estimate during each stance phase (IC to TO). PTA_{ankle_x} and PTA_{ankle_y} were defined as $a_{free,ankle_x}$ and $a_{free,ankle_y}$ at the time instant of max(PTA_{ankle_z}), respectively. PTA_{IMU_z} was taken as the peak value of a_{IMU_z} during the stance phase (IC to TO), PTA_{IMU_x} and PTA_{IMU_y} were defined as a_{IMU_x} and a_{IMU_y} at the time instant of max(a_{IMU_z}), respectively. All individual acceleration components on the right side of Equations 2-4 were evaluated at the time instant of max(a_{IMU_z}).

Area under curve: the impulse. *The time integrals of a_{IMU_z} and $a_{free,ankle_z}$ were taken to obtain the area under the curve (impulse) of the axial tibial acceleration. The starting (t_1) and end point (t_2) of the integrals were defined as the sample closest to the zero-crossings during tibial impact. If there was no zero-crossing at the start, IC was taken as starting point of the impulse.*

Statistical analysis

All data was presented as mean ± standard deviation. Statistical significance was set at α = 0.05, all statistical tests were performed in IBM SPSS Statistics (IBM, Armonk, NY, USA, version 28.0.1.0).

A repeated-measures 2-way ANOVA with Bonferroni post-hoc analysis was performed to test the differences between the distal and proximal IMU location, and type of measure ($\overrightarrow{\boldsymbol{a_{IMU}}}$ or $\overrightarrow{\boldsymbol{a_{free,ankle}}}$) over three running speeds. The Greenhouse-Geisser correction was used for the correction on sphericity. Effect size was evaluated via the common ANOVA-related partial *eta*

squared (η^2), defined as small effect size for $\eta^2 < 0.06$, medium $0.06 \leq \eta^2 < 0.14$, and large for $\eta^2 \geq 0.14$ (39).

Pearson's correlation coefficient (r) was used for the relationship between peak acceleration and impulse. Here, $\pm$ ($r \geq 0.8$) is a strong correlation, $\pm$($0.5 \leq r < 0.8$) as a moderate correlation, $\pm(0.3 \leq r < 0.5)$ as a weak correlation, and $\pm(r < 0.3)$ as a negligible correlation (40). An a priori power calculation (G*Power 3.1.9.7 (41)) showed for an expected large effect size of $\eta^2 = 0.14$ (Cohen f = 0.40) and a power of 0.95 to include at least 9 participants.

RESULTS

PTA and its components (3D)

Figure 2 shows all tibial acceleration components over the complete stance phase, for the x- and z-axis in Ψ_{IMU_f} at the proximal IMU location. Table 1 and 2 show the acceleration values at both IMU locations and over all speeds for the x- and z-axis in Ψ_{IMU_f}, respectively. Contribution of the y-axis in Ψ_{IMU_f} was limited, and therefore not shown here (see Supplemental Table 1, Supplemental Digital Content, Data of y-axis in Ψ_{IMU_f}, http://links.lww.com/MSS/C891).

Axial axis (z-axis in Ψ_{IMU_f}). Table 1 shows all accelerations components in the z-axis in Ψ_{IMU_f}. PTA_{IMU_z} only increases over speed ($p<0.001$, $F = 67.62$, $\eta^2 = 0.83$) for both IMU locations. Centripetal acceleration around the y-axis increases over speed, while centripetal acceleration around the x-axis has a relatively small contribution. Distal and proximal PTA_{ankle_z} only show a significance difference over speed ($p<0.001$, $F = 90.92$, $\eta^2 = 0.87$).

Figure 3 shows the difference between PTA_{IMU_z} and PTA_{ankle_z}. Proximally, a significant difference over speed (p<0.001, F = 6.86, η^2 = 0.83), and their interaction (p<0.001, F = 57.31, η^2 =0.80) are observed. Distally, changes are observed over speed (p<0.001, F = 66.72, η^2 = 0.83), measure (p<0.001, F = 57.87, η^2 = 0.81), and their interaction (p < 0.001, F = 73.43, η^2 = 0.84).

Tangential sagittal plane axis (x-axis in Ψ_{IMU_f}). Table 2 shows all acceleration components in the x-axis in Ψ_{IMU_f}. PTA_{IMU_x} differs significantly proximally versus distally (p=0.028, F = 6.00, η^2=0.30), and their interaction (p=0.045, F = 4.41, η^2=0.24). The tangential acceleration increases over running speed, resulting in no difference in estimation of PTA_{ankle_x} from either IMU location; where PTA_{ankle_x} only decreases over running speed (p=0.027, F = 5.58, η^2=0.29, no post-hoc pair-wise significancy).

PTA_{ankle_x} shows a significant difference with PTA_{IMU_x} proximally (p<0.001, F = 112.04, η^2=0.89) and their interaction speed*measure (p=0.001, F = 13.29, η^2=0.49). Distally, the same changes are observed between PTA_{ankle_x} and PTA_{IMU_x} (p<0.001, F = 129.75, η^2=0.90), and their interaction (p=0.001, F = 9.22, η^2=0.40), but also a relatively small change in speed (p=0.047, F = 4.62, η^2=0.25, no post-hoc pair-wise significancy).

Area under curve: the impulse

Table 3 shows the impulse of a_{IMU_z} and $a_{free,ankle_z}$ for both distal and proximal IMU. Based on a_{IMU_z}, the impulse is significantly different between the distal and proximal IMU location (p<0.001, F = 236.18, η^2=0.94), over speed (p<0.001, F = 63.64, η^2=0.82), and their

interaction ($p<0.001$, $F = 27.27$, $\eta^2=0.66$). The impulse of $a_{free,ankle_z}$ is only significant over speed ($p<0.001$, $F = 199.76$, $\eta^2=0.94$).

Between a_{IMU_z} and $a_{free,ankle_z}$ proximally, there is a significant difference over speed ($p<0.001$, $F = 106.36$, $\eta^2=0.88$) and their interaction measure*speed ($p<0.001$, $F = 75.12$, $\eta^2=0.84$). Distally, there is a difference over speed ($p<0.001$, $F = 113.40$, $\eta^2=0.89$), measure ($p<0.001$, $F = 194.80$, $\eta^2=0.93$), and their interaction ($p<0.001$, $F = 48.67$ $\eta^2=0.78$).

Figure 4 shows the mean impulse (from $a_{free,ankle_z}$) and mean PTA_{ankle_z} for every participant, based on the proximal and distal IMU, including the Pearson correlation coefficient at each speed. Based on the distal IMU, PTA and impulse showed a moderate correlation, $r = 0.64$ at 2.8 ms^{-1}, $r = 0.52$ at 3.3 ms^{-1}, and $r = 0.64$ at 3.9 ms^{-1}. A moderate to strong correlation was found based on the proximal IMU, with $r = 0.84$ at 2.8 ms^{-1}, $r = 0.73$ at 3.3 ms^{-1}, and $r = 0.79$ at 3.9 ms^{-1}.

DISCUSSION

The aim of this study was to evaluate all 3D tibial acceleration components over two different sensor locations and three running speeds (2.8, 3.3, 3.9 $m \cdot s^{-1}$), to show the contribution of angular velocity and angular acceleration in the 3D PTA estimate during running. Furthermore, the impulse of the tibial acceleration was evaluated as a more robust surrogate measure for impact load while using an IMU.

Axial peak accelerations measured by the distal IMU-accelerometer (a_{IMU_z}) were slightly higher compared with the proximal IMU-accelerometer on a group-level, however, there was no significant difference found between both IMU locations over all speeds (Table 1). This indicates that it did not matter here where the IMU was attached, but this is in contrast with previous literature (6,16,17). Lucas-Cuevas et al. (6) did find a significant difference between a distal and proximal location at 2.2, 2.8, and 3.3 $m \cdot s^{-1}$. Accelerometers were attached close to the distal end and to the antero-medial aspect of the tibia, however, no clear participant-specific clarification was given (6). The results of (6,16,17) show the importance of the location of the accelerometer in PTA estimates. The non-significant difference between peak proximal and distal acceleration found here, can be explained by the fact that the IMUs could be located closer to each other at the tibia, resulting in a smaller difference between the distal and proximal IMU accelerations. Another reason for a small distal versus proximal a_{IMU_z} difference is that four participants showed a higher proximal peak value compared to the distal peak value (see Supplemental Table 2, Supplemental Digital Content, Differences between distal and proximal subject-specific PTA and impulse values, http://links.lww.com/MSS/C891). Tissue-artefacts or muscle contractions could influence the measurements. However, the IMUs were tightly fitted and did not get loose from the tibia during the measurements, still, external factors can influence the peak acceleration values distally and proximally as shown here. The majority of PTA studies do only use one sensor on the tibia (e.g., (2)), therefore not directly evaluating external factors as there is no reference sensor on the same segment. Therefore, it is unknown how reliable PTA measurements with IMUs are in previous literature due to the influence of these external factors. Furthermore, the generally lower sample frequency of an IMU compared with high-sampling accelerometers could result in missing the actual peak tibial acceleration value, however, this should occur on

both IMU locations. The result of this study indicates that peak accelerations taken at the tibia could not always be trustworthy and PTA based on a single sample could be highly influenced by external and sensor-related factors, providing evidence for shifting interest towards more robust measurement, like the impulse.

Centripetal acceleration around the y-axis in Ψ_{IMU_f} showed a difference between IMU locations and over speed (Table 1), confirming the importance of the inclusion of centripetal acceleration over different speeds. Lafortune et al. (18) found a centripetal acceleration of approximately 50 m·s^{-2} for runners, five times higher than found here. Their rotation arm of 0.42 m on average was almost 1.5 times the rotation arm in this study. However, this does not explain the big difference. Lake et al. (22) corrected the impact peak by +1.5 to +3g for their two participants due to gravitational and centripetal acceleration, which implies a centripetal acceleration of approximately 25 to 40 m·s^{-2}. In this study, the angular velocity measured here was in the same range of similar joint angular velocities (42). Running overground compared to running on a treadmill, specific running technique of the participants or the use of optical motion capture for estimation of angular velocity in these studies could be factors for this difference, but this remains not fully understood.

The increment of centripetal acceleration over increasing speed causes that the PTA_{ankle_z} does differ from the PTA_{IMU_z} over different speeds, as hypothesized. At the proximal IMU location, the PTA_{ankle_z} and PTA_{IMU_z} are approximately the same (Table 1), as the centripetal acceleration value is similar to the gravitational acceleration. Although differences are small, PTA seems to show a steeper slope of increment over different running speeds as centripetal

acceleration increases over speed compared to the constant gravitational acceleration. The significant interaction speed*measure ($p<0.001$) underlines this behaviour at the proximal IMU location. The distal IMU location showed a bigger systematic offset between PTA_{ankle_z} and PTA_{IMU_z}, caused by a smaller centripetal acceleration (between 3.96-6.29 $m \cdot s^{-2}$) compared to the proximal IMU location. These results suggest that measuring on a proximal IMU location is closer towards the actual impact PTA compared with a distal IMU location due to this larger offset. Overall, the difference between PTA_{ankle_z} and PTA_{IMU_z} was found, but expected to be greater, as described by Lafortune et al. (18).

To the author's knowledge, tangential acceleration has not been evaluated in previous PTA studies, but does have a relevant contribution in the x-axis in $\Psi_{\mathrm{IMU_f}}$ for the acceleration during running (Table 2). Inclusion of tangential acceleration makes PTA in the x-axis in $\Psi_{\mathrm{IMU_f}}$ more negative for both IMU locations, which can be expected during the braking phase at impact, where the forward-directed tangential acceleration of the tibia cancels out this braking acceleration. Especially in studies investigating the 3D vector norm of tibial acceleration take this tangential acceleration factor into account and are therefore likely to misinterpret the PTA. Thus, the braking impact acceleration is actually strongly negative compared to what an accelerometer actually measures.

The inclusion of angular velocity and angular acceleration is needed to accurately estimate PTA by impact with the ground only. This is substantiated by the slightly different slopes of PTA_{ankle_z} compared to PTA_{IMU_z} over different speeds, and the difference in PTA_{ankle_z}versus PTA_{IMU_z} distally. Still, accelerometers are often placed distally (20–22), which

results in an offset between PTA_{IMU_z} and $PTA_{z_{ankle}}$. Furthermore, for both the proximal and distal IMU location, the PTA_{ankle_z} showed a steeper increment over different running speed compared to PTA_{IMU_z}. This makes inclusion of centripetal and tangential acceleration an interesting finding for more accurate PTA estimates over different speeds, although the contributions are smaller compared to previous findings (18,22).

The application of Rigid Body Kinematics to take into account centripetal and tangential accelerations depends on angular velocities and therefore on IMUs: the question rises if such a sensor can measure accurately enough since they generally have a lower sample frequency. A lower sampling frequency allows for prolonged measurement of multiple parameters (e.g., sensor acceleration, angular velocity and sensor orientation) indoors and outdoors (2), but might have limitations for the assessment of the exact peak in PTA. The inclusion of angular velocity and angular accelerations seems necessary to estimate tibial acceleration by impact only, however. An option to counteract this is to look at the impulse: the impulse has already its applications in force impact estimates of GRF (28) or pressure insoles (29) as mechanical impulse. The impulse used here, the time integral of tibial acceleration, ignores the effective mass that is accelerated. However, the time integral includes not only magnitude but also the time interval over which it acts. The impulse seems therefore more robust against external factors and less dependent on sampling frequency. The impulse under a_{IMU_z} curve showed a significant difference over speed ($p < 0.001$, $F = 63.64$, $\eta^2 = 0.82$), location ($p < 0.001$, $F = 236.18$, $\eta^2 = 0.94$), and their interaction speed*location ($p < 0.001$, $F = 27.27$, $\eta^2 = 0.66$) between the proximal and distal location. The four participants showing higher proximal peak acceleration values compared to the distal IMU, did show a larger impulse distally (see Supplemental Table 2, Supplemental Digital Content,

Differences between distal and proximal subject-specific PTA and impulse values, http://links.lww.com/MSS/C891) as one would expect: a larger peak acceleration is expected distally as there is less influence of centripetal accelerations. As the PTA values obtained here do not always show this behaviour, but impulse does for all participants, underlies that a single peak value can probably be trusted less compared to the impulse.

The impulse based on a_{IMU_z} does show a significant difference between IMU location: this relates to the findings of Lucas-Cuevas et al. (6) based on distal and proximal PTA. The impulse of $a_{free,ankle_z}$ did not show a significant difference between IMU locations, as expected, as they both are translated towards the ankle based on RBK. Pearson correlations coefficients showed moderate to strong correlations between impulse and PTA, indicating that impulse give relatable results compared to PTA. Including the impulse instead of only one peak value seems, as hypothesized, a more robust estimate of tibial impact load as surrogate measure and should be investigated in further research.

The sample frequency used here with IMUs (240 Hz) can, as a result, be seen as a limitation as papers investigating (peak) impact acceleration frequently usually use accelerometers with a high sample frequency of 1000 Hz or higher (14). This high frequency is, based on the papers mentioned in the review of Sheerin et al. (14), chosen to detect the peak value accurately. However, Reenalda et al. (2) found that 96.3% of the impact acceleration signal is below 50 Hz, measured with a 1200 Hz accelerometer. This indicates that a sample frequency of 240 Hz can theoretically detect frequencies up to 120 Hz. Furthermore, Mitschke et al. (27) defined that at least a sample frequency of 200 Hz is needed to identify peak tibial acceleration

values. Although the sample frequency is lower in IMUs compared with single accelerometers, the need for angular velocity in PTA estimates makes the use of IMUs more suited to find the impact PTA. Still, peak values are not always correctly detected for both IMU locations, creating doubt about the minimal sample frequency needed (27) and the use of single peak acceleration values in surrogate tibial load estimates versus the use of the impulse.

Future research could focus on using more advanced IMUs with higher sample frequencies and less disturbance from external factors (e.g., tissue-artefact, muscle contraction). Furthermore, the impulse outcome could include the effective mass to obtain a better estimate of mechanical impulse during running (28). Impulse could also be directly compared with, for example, the average loading rate of a force plate, or in relation to tibial bone load estimate including muscle and external forces (40). Externally measured parameters only provide information about one part of the tibial bone loading estimates. Other factors like muscle forces acting on the tibia and the bending and deformation of the tibia under impact should also be investigated to get a better insight into the etiology of running related injuries of the tibia (9–13). This could eventually contribute to injury prevention. The proposed method could potentially be used in real-time feedback application based on IMUs. For this, the orientation estimation as used in this study (based on (36)) needs to be updated for quasi-real time orientation estimation. This means that the time-invariant functional axis used for the tibia IMUs needs to be updated and validated to a time-variant functional axis, as this functional axis can vary for every stride when not running on a treadmill, or can vary even within a stride. Future research should investigate and validate the use of a time-variant functional axis between and within strides. Furthermore, estimates of the internal forces need to be included.

CONCLUSIONS

The importance of centripetal and tangential acceleration in the estimation of PTA was shown here during treadmill running at different speeds, where significant differences were found between PTA_{ankle_z} and PTA_{IMU_z} at two IMU locations. However, the impulse seems to be a more robust parameter to obtain knowledge about the tibial load during running, as the peak IMU-accelerometer values are not always detected correctly. It is suggested to use an accelerometer with high sampling frequency at the medial or lateral malleolus to avoid centripetal and tangential accelerations, or to use an IMU with high sampling frequency at a known location on the tibia to be able to accurately correct for centripetal and tangential acceleration. Concluding, tibial acceleration should be corrected by centripetal, tangential and gravitational accelerations. It is suggested to use the impulse of $a_{free,ankle_z}$ to obtain a surrogate measure for tibial bone load. As such, the future might lie in adding centripetal and tangential components when the sampling frequency is sufficient and in evaluating at the impulse.

Acknowledgements and conflict of interest

This project is funded by a general research fund of the University of Twente, Enschede, The Netherlands. All authors declare no conflict of interest. The results of the study are presented clearly, honestly, and without fabrication, falsification, or inappropriate data manipulation. The results of the present study do not constitute endorsement by the American College of Sports Medicine.

REFERENCES

1. Derrick TR, Dereu D, McLean SP. Impacts and kinematic adjustments during an exhaustive run. *Med Sci Sports Exerc.* 2002;34(6):998–1002.
2. Reenalda J, Maartens E, Buurke JH, Gruber AH. Kinematics and shock attenuation during a prolonged run on the athletic track as measured with inertial magnetic measurement units. *Gait Posture.* 2019;68:155–60.
3. Clansey AC, Hanlon M, Wallace ES, Lake MJ. Effects of fatigue on running mechanics associated with tibial stress fracture risk. *Med Sci Sports Exerc.* 2012;44(10):1917–23.
4. Mizrahi J, Verbitsky O, Isakov E, Daily D. Effect of fatigue on leg kinematics and impact acceleration in long distance running. *Hum Mov Sci.* 2000;19(2):139–51.
5. García-Pérez JA, Pérez-Soriano P, Llana Belloch S, Lucas-Cuevas AG, Sánchez-Zuriaga D. Effects of treadmill running and fatigue on impact acceleration in distance running. *Sports Biomech.* 2014;13(3):259–66.
6. Lucas-Cuevas AG, Encarnación-Martínez A, Camacho-García A, Llana-Belloch S, Pérez-Soriano P. The location of the tibial accelerometer does influence impact acceleration parameters during running. *J Sports Sci.* 2017;35(17):1734–8.
7. Pohl MB, Mullineaux DR, Milner CE, Hamill J, Davis IS. Biomechanical predictors of retrospective tibial stress fractures in runners. *J Biomech.* 2008;41(6):1160–5.
8. Milner CE, Ferber R, Pollard CD, Hamill J, Davis IS. Biomechanical factors associated with tibial stress fracture in female runners. *Med Sci Sports Exerc*. 2006;38(2):323-8.
9. Matijevich ES, Scott LR, Volgyesi P, Derry KH, Zelik KE. Combining wearable sensor signals, machine learning and biomechanics to estimate tibial bone force and damage during running. *Hum Mov Sci.* 2020;74:102690.

10. Zandbergen MA, Ter Wengel XJ, van Middelaar RP, Buurke JH, Veltink PH, Reenalda J. Peak tibial acceleration should not be used as indicator of tibial bone loading during running. *Sports Biomech.* 2023;1–18.
11. Yang PF, Sanno M, Ganse B, et al. Torsion and antero-posterior bending in the in vivo human tibia loading regimes during walking and running. *PLoS One.* 2014;9(4):e94525.
12. Haider IT, Baggaley M, Edwards WB. Subject-specific finite element models of the tibia with realistic boundary conditions predict bending deformations consistent with in vivo measurement. *J Biomech Eng.* 2019;142(2):021010.
13. Khassetarash A, Haider I, Baggaley M, Edwards WB. Tibial strains during prolonged downhill running: a finite element analysis. *J Biomech Eng.* 2022;145(4):041007.
14. Sheerin KR, Reid D, Besier TF. The measurement of tibial acceleration in runners - a review of the factors that can affect tibial acceleration during running and evidence-based guidelines for its use. *Gait Posture.* 2019;67:12–24.
15. Nigg BM, Cole GK, Brüggemann GP. Impact forces during heel-toe running. *J Appl Biomech.* 1995;11(4):407–32.
16. Xiang L, Gu Y, Rong M, et al. Shock acceleration and attenuation during running with minimalist and maximalist shoes: a time- and frequency-domain analysis of tibial acceleration. *Bioengineering (Basel).* 2022;9(7):322.
17. Ryu S, Lee YS, Park SK. Impact signal differences dependent on the position of accelerometer attachment and the correlation with the ground reaction force during running. *Int J Precis Eng Manuf.* 2021;22(10):1791–8.
18. Lafortune MA, Hennig EM. Contribution of angular motion and gravity to tibial acceleration. *Med Sci Sports Exerc.* 1991;23(3):360–3.

19. Ginsberg JH. *Advanced Engineering Dynamics.* 2nd ed. New York: Cambridge University Press; 1995. 462 p.
20. Camelio K, Gruber AH, Powell DW, Paquette MR. Influence of prolonged running and training on tibial acceleration and movement quality in novice runners. *J Athl Train.* 2020;55(12):1292–9.
21. Waite N, Goetschius J, Lauver JD. Effect of grade and surface type on peak tibial acceleration in trained distance runners. *J Appl Biomech.* 2020;37(1):2–5.
22. Lake MJ, Greenhalgh A. Impact shock measurements during running: correction for angular motion of the shank is necessary. In: 7th Symposium on Footwear Biomechanics. Cleveland, USA; 2005.
23. Verbitsky O, Mizrahi J, Voloshin A, Treiger J, Isakov E. Shock transmission and fatigue in human running. *J Appl Biomech.* 1998;14(3):300–11.
24. Mercer JA, Vance J, Hreljac A, Hamill J. Relationship between shock attenuation and stride length during running at different velocities. *Eur J Appl Physiol.* 2002;87(4–5):403–8.
25. Clarke TE, Cooper LB, Hamill CL, Clark DE. The effect of varied stride rate upon shank deceleration in running. *J Sports Sci.* 1985;3(1):41–9.
26. Camomilla V, Bergamini E, Fantozzi S, Vannozzi G. Trends supporting the in-field use of wearable inertial sensors for sport performance evaluation: a systematic review. *Sensors (Basel).* 2018;18(3):873.
27. Mitschke C, Zaumseil F, Milani TL. The influence of inertial sensor sampling frequency on the accuracy of measurement parameters in rearfoot running. *Comput Methods Biomech Biomed Engin.* 2017;20(14):1502–11.

28. Addison BJ, Lieberman DE. Tradeoffs between impact loading rate, vertical impulse and effective mass for walkers and heel strike runners wearing footwear of varying stiffness. *J Biomech.* 2015;48(7):1318–24.
29. Fu W, Fang Y, Liu DMS, Wang L, Ren S, Liu Y. Surface effects on in-shoe plantar pressure and tibial impact during running. *J Sport Health Sci.* 2015;4(4):384–90.
30. Meardon SA, Derrick TR, Willson JD, et al. Peak and per-step tibial bone stress during walking and running in female and male recreational runners. *Am J Sports Med.* 2021;49(8):2227–37.
31. Glassbrook DJ, Fuller JT, Alderson JA, Wills JA, Doyle TLA. Changes in acceleration load as measured by inertial measurement units manifest in the upper body after an extended running task. *J Sports Sci.* 2022;40(13):1467–75.
32. Scheltinga BL, Usta H, Reenalda J, Buurke JH. Estimating vertical ground reaction force during running with 3 inertial measurement units. *J Biomed Eng Biosci.* 2022;9(1):31–8.
33. Gruber AH, Boyer KA, Derrick TR, Hamill J. Impact shock frequency components and attenuation in rearfoot and forefoot running. *J Sport Health Sci.* 2014;3(2):113–21.
34. van Melick N, Meddeler BM, Hoogeboom TJ, Nijhuis-van der Sanden MWG, van Cingel REH. How to determine leg dominance: the agreement between self-reported and observed performance in healthy adults. *PLoS One.* 2017;12(12):e0189876.
35. Radzak KN, Putnam AM, Tamura K, Hetzler RK, Stickley CD. Asymmetry between lower limbs during rested and fatigued state running gait in healthy individuals. *Gait Posture.* 2017;51:268–74.

36. Zandbergen MA, Reenalda J, van Middelaar RP, Ferla RI, Buurke JH, Veltink PH. Drift-free 3D orientation and displacement estimation for quasi-cyclical movements using one inertial measurement unit: application to running. *Sensors (Basel)*. 2022;22(3):956.
37. Falbriard M, Meyer F, Mariani B, Millet GP, Aminian K. Accurate estimation of running temporal parameters using foot-worn inertial sensors. *Front Physiol.* 2018;9:610.
38. Karatsidis A, Bellusci G, Schepers HM, de Zee M, Andersen MS, Veltink PH. Estimation of ground reaction forces and moments during gait using only inertial motion capture. *Sensors (Basel).* 2016;17(1):75.
39. Cohen J. *Statistical Power Analysis for the Behavioral Sciences.* 2nd ed. Hillsdale, N.J: L. Erlbaum Associates; 1988. 567 p.
40. Matijevich ES, Branscombe LM, Scott LR, Zelik KE. Ground reaction force metrics are not strongly correlated with tibial bone load when running across speeds and slopes: Implications for science, sport and wearable tech. *PLoS One.* 2019;14(1):e0210000.
41. Faul F, Erdfelder E, Lang AG, Buchner A. G*Power 3: A flexible statistical power analysis program for the social, behavioral, and biomedical sciences. *Behav Res Methods.* 2007;39(2):175–91.
42. Sinclair J, Hobbs SJ, Protheroe L, Edmundson CJ, Greenhalgh A. Determination of gait events using an externally mounted shank accelerometer. 2013;29(1):118–22.

FIGURE LEGENDS

Figure 1: Distal (above ankle) and proximal (below knee) IMU on the tibia of the dominant leg. Left: frontal plane view, IMUs shown as originally attached to the tibia in Ψ_{IMU_p} and Ψ_{IMU_d}. Right: sagittal plane view, IMU CS shown as rotated based on PCA (see 'Data Processing') into $\Psi_{IMU_{p_f}}$ and $\Psi_{IMU_{d_f}}$.

Figure 2: All tibial acceleration components from Equation 2 & 4 visualized in the complete stance phase for one participant at 3.3 $m \cdot s^{-1}$ at the proximal IMU location. Axes shown in the Ψ_{IMU_f} CS. Mean over 30 strides visualized with a shaded standard deviation. Impulse window also visible.

Figure 3: Difference of $PTA_{z_{ankle}}$ vs. $PTA_{z_{IMU}}$ based on the proximal and distal IMU location.

Figure 4: PTA estimates versus the impulse, as mean over 30 strides of each participant. Data shown for 2.8, 3.3, 3.9 $m \cdot s^{-1}$ including Pearson correlation (r) for each speed.

SUPPLEMENTAL DIGITAL CONTENT

SDC 1: Supplemental Digital Content.docx

Figure 1

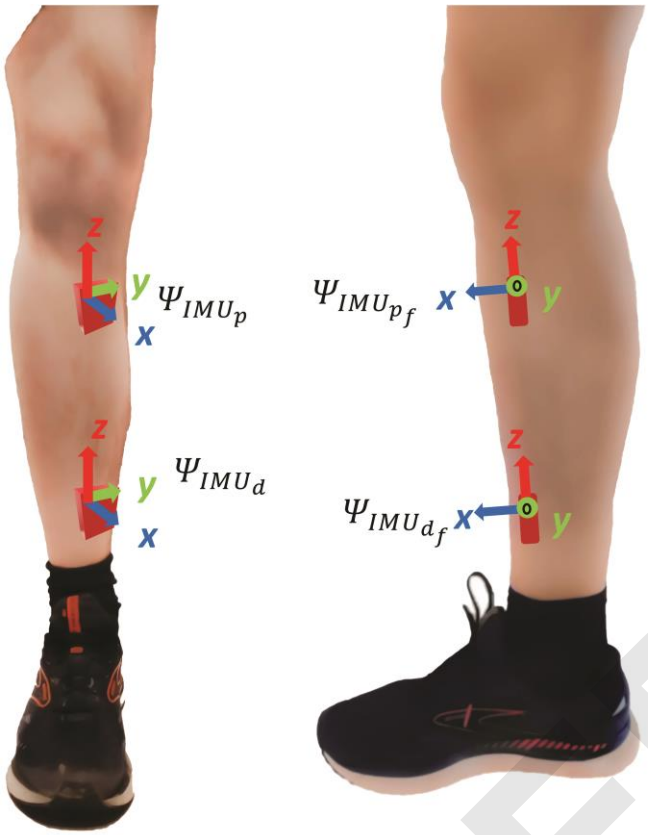

Figure 2

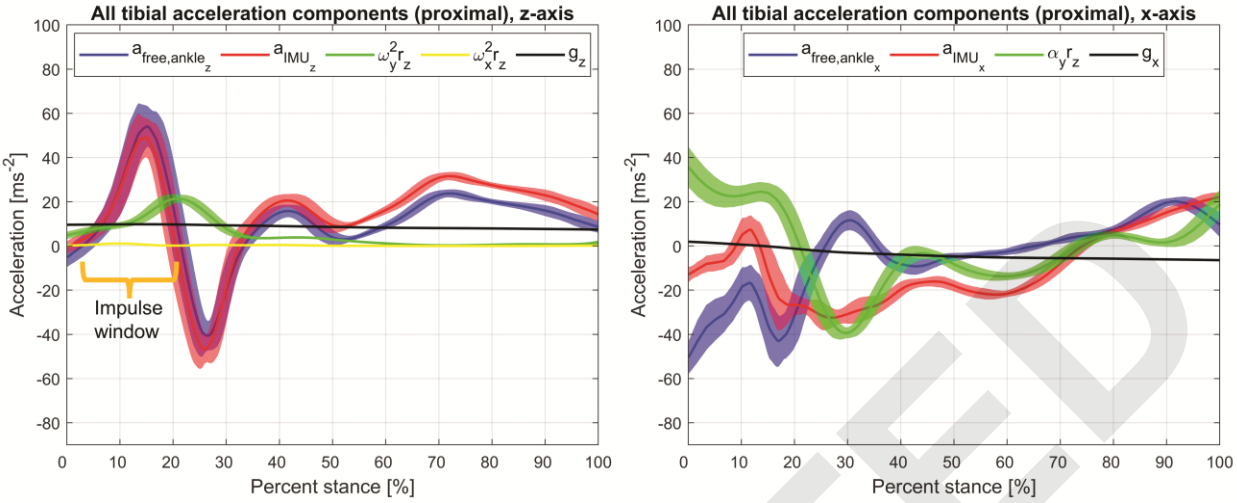

Figure 3

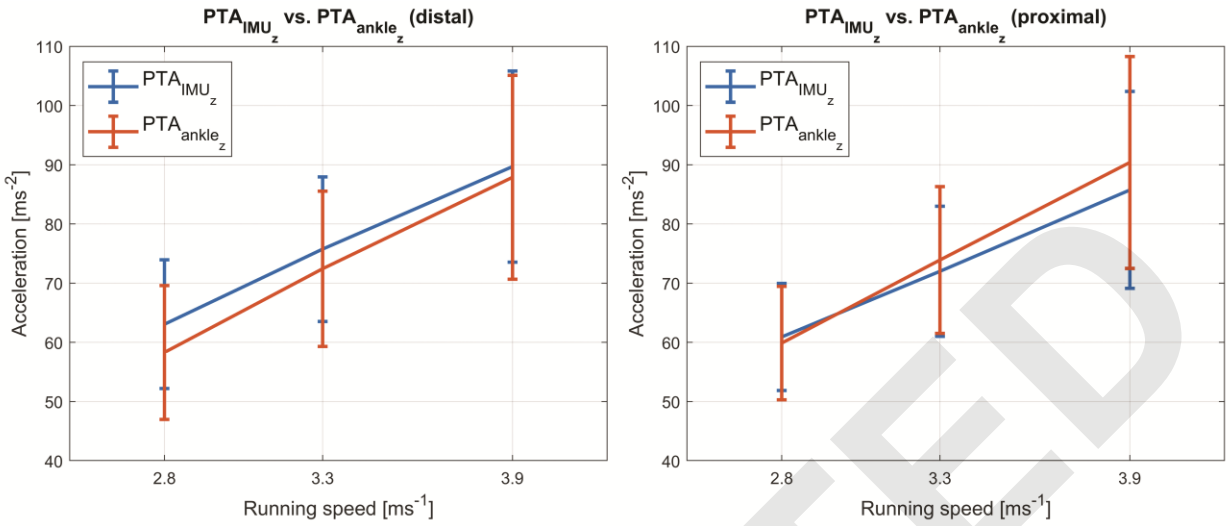

Figure 4

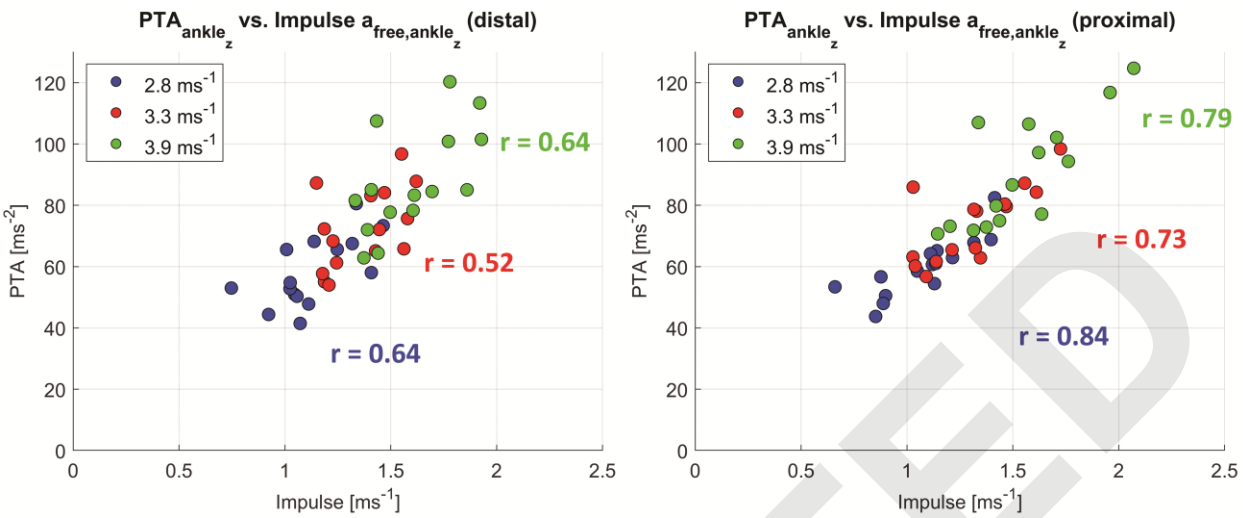

Table 1: Acceleration components as mentioned in Equation 4, based on both IMU locations.

Axial axis (z-axis in Ψ_{IMU_f})

	PROXIMAL IMU			***DISTAL IMU***		
	2.8 m·s^{-1}	***3.3 m·s^{-1}***	***3.9 m·s^{-1}***	***2.8 m·s^{-1}***	***3.3 m·s^{-1}***	***3.9 m·s^{-1}***
PTA_{IMU_z} ($m{\cdot}s^{-2}$)	60.92 $^{*\,a}$ ± 9.05	72.01 $^{*\,a}$ ± 10.98	85.74 $^{*\,a}$ ± 16.63	63.07 $^{*\,w\,a}$ ± 10.86	75.74 $^{*\,w\,a}$ ± 12.21	89.69 $^{*\,w\,a}$ ± 16.15
$\omega_y^2\, r_z$ ($m{\cdot}s^{-2}$)	7.69 ± 2.75	10.24 ± 3.92	12.69 ± 4.87	3.96 ± 1.02	5.05 ± 1.19	6.29 ± 1.75
$\omega_x^2\, r_z$ ($m{\cdot}s^{-2}$)	0.96 ± 0.76	1.29 ± 0.97	1.55 ± 1.19	0.24 ± 0.13	0.33 ± 0.24	0.40 ± 0.23
g_z ($m{\cdot}s^{-2}$)	9.73 ± 0.09	9.71 ± 0.11	9.71 ± 0.11	9.73 ± 0.10	9.71 ± 0.11	9.71 ± 0.11
PTA_{ankle_z} ($m{\cdot}s^{-2}$)	59.89 $^{*\,a}$ ± 9.58	73.91 $^{*\,a}$ ± 12.38	90.38 $^{*\,a}$ ± 17.89	58.29 $^{*\,w\,a}$ ± 11.29	72.43 $^{*\,w\,a}$ ± 13.11	87.89 $^{*\,w\,a}$ ± 17.22

Values are reported as mean ± SD. PTA_{IMU_z} and PTA_{ankle_z} are the values of max(a_{IMU_z}) and max$\left(a_{free,ankle_z}\right)$, respectively. * indicates significant difference over speed, ^{x} between IMU locations, ^{h} shows significant interaction location*speed. ^{w} shows significant difference between measure $\mathrm{PTA}_{\mathrm{IMU_z}}$ and $\mathrm{PTA}_{\mathrm{ankle_z}}$, ^{a} shows significant interaction measure*speed.

Table 2: Acceleration components as mentioned in Equation 2, based on both IMU locations.

Tangential sagittal plane axis (x-axis in Ψ_{IMU_f})

	PROXIMAL IMU			***DISTAL IMU***		
	2.8 m·s^{-1}	***3.3 m·s^{-1}***	***3.9 m·s^{-1}***	***2.8 m·s^{-1}***	***3.3 m·s^{-1}***	***3.9 m·s^{-1}***
$\boldsymbol{PTA_{IMU_x}}$ ($m{\cdot}s^{-2}$)	-0.45 $^{x\,h\,w\,a}$ ± 21.30	-0.61 $^{x\,h\,w\,a}$ ± 24.75	0.73 $^{x\,h\,w\,a}$ ± 23.73	-9.30 $^{x\,h\,w\,a}$ ± 25.75	-16.32 $^{x\,h\,w\,a}$ ± 26.81	-23.11 $^{x\,h\,w\,a}$ ± 31.70
$\boldsymbol{\alpha_y^2\, r_z}$ ($m{\cdot}s^{-2}$)	17.94 ± 7.38	22.35 ± 8.86	24.93 ± 10.58	8.34 ± 2.51	9.40 ± 2.33	10.26 ± 2.84
$\boldsymbol{g_x}$ ($m{\cdot}s^{-2}$)	-0.09 ± 1.14	0.14 ± 1.19	0.38 ± 1.05	-0.14 ± 1.16	0.10 ± 1.21	0.33 ± 1.10
$\boldsymbol{PTA_{ankle_x}}$ ($m{\cdot}s^{-2}$)	-19.45 $^{w\,a}$ ± 20.35	-24.60 $^{w\,a}$ ± 24.80	-26.36 $^{w\,a}$ ± 28.41	-17.97 $^{w\,a}$ ± 25.65	-26.49 $^{w\,a}$ ± 25.71	-34.26 $^{w\,a}$ ± 30.32

Values are reported as mean ± SD. PTA_{IMU_x} is the value of a_{IMU_x} at the time instant of max(a_{IMU_z}), PTA_{ankle_x} is the value of $a_{free,ankle_x}$ at time instant of max($a_{free,ankle_z}$). * indicates significant difference over speed, ^{x} between IMU locations, ^{h} shows significant interaction location*speed. ^{w} shows significant difference between measure $\mathrm{PTA}_{\mathrm{IMU}_x}$ and $\mathrm{PTA}_{\mathrm{ankle}_x}$, ^{a} shows significant interaction measure*speed.

Table 3: Area under the curve (impulse) of a_{IMU_z} and $a_{free,ankle_z}$, based on both IMU locations.

	PROXIMAL IMU			***DISTAL IMU***		
	2.8 m·s^{-1}	***3.3 m·s^{-1}***	***3.9 m·s^{-1}***	***2.8 m·s^{-1}***	***3.3 m·s^{-1}***	***3.9 m·s^{-1}***
Impulse a_{IMU_z} *(m·s^{-1})*	1.16$^{*\,x\,h\,a}$ ± 0.20	1.30$^{*\,x\,h\,a}$ ± 0.18	1.43$^{*\,x\,h\,a}$ ± 0.21	1.40$^{*\,x\,h\,w\,a}$ ± 0.20	1.59$^{*\,x\,h\,w\,a}$ ± 0.18	1.78$^{*\,x\,h\,w\,a}$ ± 0.22
Impulse $a_{free,ankle_z}$ *(m·s^{-1})*	1.08$^{*\,a}$ ± 0.21	1.31$^{*\,a}$ ± 0.22	1.54$^{*\,a}$ ± 0.26	1.13$^{*\,w\,a}$ ± 0.19	1.36$^{*\,w\,a}$ ± 0.17	1.60$^{*\,w\,a}$ ± 0.21

Values are reported as mean ± SD. * indicates significant difference over speed, ^{x} between IMU locations, ^{h} shows significant interaction location*speed. ^{w} shows significant difference between measure a_{IMU_z} and $a_{free,ankle_z}$, ^{a} shows significant interaction measure*speed.

Supplemental Digital Content

Gravitational acceleration determination & alignment $\Psi_{IMU_{p_f}}$ and $\Psi_{IMU_{d_f}}$

3D gravitational acceleration, $\vec{g}$ (m·s^{-2}), was obtained at the proximal IMU location as the difference between the IMU-measured acceleration (including gravity) and gravity-free acceleration. Gravity-free acceleration was obtained by rotating the IMU-measured acceleration from $\Psi_{IMU_{p_f}}$ towards a world-fixed CS with the Drift-Free Orientation & Displacement (DFOD) algorithm (1) , subtracted 9.81 m·s^{-2} in the vertical direction, and rotated back towards $\Psi_{IMU_{p_f}}$. The same method was applied to $\Psi_{IMU_{d_f}}$ to obtain 3D gravitational acceleration at the distal IMU location.

The orientation of $\Psi_{IMU_{p_f}}$ and $\Psi_{IMU_{d_f}}$ was not exactly aligned due to potential small differences in sensor attachment or in DFOD. For an aligned CS of the distal and proximal IMU, it is assumed that $\vec{g}$ (m·s^{-2}) should be identical for both IMUs. $\vec{g}_{prox}$ and $\vec{g}_{dist}$ were used to rotate $\Psi_{IMU_{d_f}}$ in line with $\Psi_{IMU_{p_f}}$ for every time sample t, based on the Euler-Rodrigues formula (2) (Equation 3). To do that, the cross-product of $\vec{g}_{prox}$ and $\vec{g}_{dist}$, divided by its respective norm, $\vec{k}(t)$, was taken in Equation 1:

$$\vec{k}(t) = \frac{\vec{g}_{dist}(t)}{\|\vec{g}_{dist}(t)\|} \times \frac{\vec{g}_{prox}(t)}{\|\vec{g}_{prox}(t)\|} \quad [1]$$

Based on this cross product $\vec{k}(t)$, a time-dependent rotation matrix $\boldsymbol{R_k}(t)$ can be formed (Equation 2):

$$\boldsymbol{R_k}(t) = \begin{bmatrix} 0 & -k_z(t) & k_y(t) \\ k_z(t) & 0 & -k_x(t) \\ -k_y(t) & k_x(t) & 0 \end{bmatrix} \quad [2]$$

Equation 2 is used to find the time-dependent rotation matrix $\boldsymbol{R}_{\boldsymbol{dist}}^{\boldsymbol{prox}}(t)$:

$$\boldsymbol{R}_{\boldsymbol{dist}}^{\boldsymbol{prox}}(t) = \boldsymbol{I} + \boldsymbol{R}_{\boldsymbol{k}}(t) + \boldsymbol{R}_{\boldsymbol{k}}^{\boldsymbol{2}}(t)\frac{1-(\vec{\boldsymbol{g}}_{\boldsymbol{dist}}(t)\cdot\vec{\boldsymbol{g}}_{\boldsymbol{prox}}(t))}{\|\vec{\boldsymbol{k}}(\boldsymbol{t})\|^2} \quad [3]$$

With $\boldsymbol{I}$ as identity matrix. Data in $\Psi_{IMU_{d_f}}$ is then multiplied by $\boldsymbol{R}_{\boldsymbol{dist}}^{\boldsymbol{prox}}(t)$ to be aligned with $\Psi_{IMU_{p_f}}$. Therefore, $\Psi_{IMU_{p_f}}$ and $\Psi_{IMU_{d_f}}$ are now assumed identical over time and defined as Ψ_{IMU_f} in the remainder of this paper.

References

1. Zandbergen MA, Reenalda J, van Middelaar RP, Ferla RI, Buurke JH, Veltink PH. Drift-Free 3D Orientation and Displacement Estimation for Quasi-Cyclical Movements Using One Inertial Measurement Unit: Application to Running. Sensors. 2022 Jan;22(3):956.

2. Dai JS. Euler–Rodrigues formula variations, quaternion conjugation and intrinsic connections. Mech Mach Theory. 2015 Oct 1;92:144–52.

Supplemental Table 1: Tangential frontal plane axis values (y-axis in Ψ_{IMU_f}). Acceleration components as mentioned in Equation 3, based on both IMU locations. No statistical testing was performed on this data due to a limited contribution.

Tangential frontal plane axis (y-axis in Ψ_{IMU_f})

	PROXIMAL			***DISTAL***		
	2.8 m·s^{-1}	***3.3 m·s^{-1}***	***3.9 m·s^{-1}***	***2.8 m·s^{-1}***	***3.3 m·s^{-1}***	***3.9 m·s^{-1}***
$\boldsymbol{PTA_{IMU_y}}$ ($m{\cdot}s^{-2}$)	-2.02 ± 13.15	-6.25 ± 14.00	-7.77 ± 16.75	2.11 ± 21.68	-0.05 ± 21.23	2.35 ± 20.05
$\boldsymbol{\alpha_x^2\, r_z}$ ($m{\cdot}s^{-2}$)	-0.41 ± 9.53	0.00 ± 8.82	-0.37 ± 8.92	-2.26 ± 4.80	-2.00 ± 5.05	-2.33 ± 5.00
$\boldsymbol{g_y}$ ($m{\cdot}s^{-2}$)	-0.30 ± 0.39	-0.42 ± 0.58	-0.46 ± 0.67	-0.29 ± 0.40	-0.40 ± 0.60	-0.45 ± 0.69
$\boldsymbol{PTA_{ankle_y}}$ ($m{\cdot}s^{-2}$)	-1.27 ± 14.65	-5.68 ± 14.45	-7.01 ± 16.72	4.46 ± 19.42	2.34 ± 18.84	4.99 ± 18.58

Values are reported as mean ± SD. PTA_{IMU_y} is the value of a_{IMU_y} at the time instant of max(a_{IMU_z}), PTA_{ankle_y} is the value of $a_{free,ankle_y}$ at time instant of max($a_{free,ankle_z}$).

Supplemental Table 2: Differences between distal and proximal IMU of the peak acceleration value (axial axis and vector norm) and impulse.

The difference between distal and proximal IMU values (proximal minus distal) of subject-specific PTA_{IMU_z} in z-axis of Ψ_{IMU_f}, its 3D vector norm, and the impulse.

	PTA_{IMU_z} ($m \cdot s^{-2}$)			Norm PTA_{IMU} ($m \cdot s^{-2}$)			Impulse ($m \cdot s^{-1}$)		
#	*2.8* $m \cdot s^{-1}$	*3.3* $m \cdot s^{-1}$	*3.9* $m \cdot s^{-1}$	*2.8* $m \cdot s^{-1}$	*3.3* $m \cdot s^{-1}$	*3.9* $m \cdot s^{-1}$	*2.8* $m \cdot s^{-1}$	*3.3* $m \cdot s^{-1}$	*3.9* $m \cdot s^{-1}$
1	7.49	12.14	11.36	-12.83	-9.99	-14.93	-0.16	-0.22	-0.29
2	3.83	7.31	17.93	11.17	10.21	18.64	-0.30	-0.34	-0.35
3	2.08	3.21	7.40	-3.38	-8.00	-11.00	-0.25	-0.23	-0.35
4	-1.55	-6.68	-12.46	-4.28	-9.17	-14.34	-0.19	-0.27	-0.34
5	-11.37	-5.46	-0.16	-4.70	-0.69	-7.24	-0.19	-0.20	-0.27
6	-17.47	-21.67	-18.96	-18.58	-22.19	-21.28	-0.35	-0.40	-0.42
7	-11.53	-12.63	-16.71	-12.46	-14.52	-20.22	-0.25	-0.29	-0.39
8	-4.66	-6.97	-8.57	-33.39	-26.34	-19.84	-0.25	-0.29	-0.31
9	-7.42	-14.72	-19.25	-13.34	-17.08	-33.38	-0.31	-0.39	-0.42
10	22.12	24.35	23.66	21.49	22.15	20.60	-0.20	-0.18	-0.15
11	-6.18	-9.81	-13.01	2.01	2.70	3.64	-0.23	-0.25	-0.32
12	0.01	0.03	0.78	3.39	5.42	2.30	-0.16	-0.20	-0.21
13	-9.74	-24.17	-31.31	-10.07	-24.37	-28.94	-0.30	-0.43	-0.58
14	7.88	8.70	7.57	-6.10	-12.19	-13.31	-0.22	-0.27	-0.37
15	-5.72	-9.54	-7.52	-12.47	-13.29	-10.16	-0.24	-0.33	-0.43
Mean ± SD	-2.15 ± 9.89	-3.73 ± 13.13	-3.95 ± 15.43	-6.24 ± 12.88	-7.82 ± 13.55	-9.96 ± 15.56	-0.24 ± 0.06	-0.29 ± 0.08	-0.35 ± 0.10

Green means distal IMU value is higher than proximal IMU value, red mean proximal IMU is higher than distal IMU value.